3D-printed 4-zone Ka-band Fresnel lens: design, fabrication, and measurement

Kyoung Ho Jeong[1], Nima Ghalichechian[1] ✉

[1]ElectroScience Laboratory, Department of Electrical and Computer Engineering, The Ohio State University, 1330 Kinnear Road, Columbus, OH, USA
✉ E-mail: ghalichechian.1@osu.edu

Abstract: A planar and thin-grooved Fresnel lens is a great candidate for gain enhancement in millimetre wave communication, imaging systems, and wireless power transfer applications. The authors report the design, fabrication, and measurement of a 3D-printed Fresnel lens, using a single material. A low-profile (1.2 λ thick) 4-zone Fresnel lens with 16 annular rings is designed with a focal length of 40 mm ($\simeq 4\lambda$) operating at 30 GHz. Authors' design consists of four-step heights with outer radius of 69 mm (6.9λ). Permittivity and loss tangent of polylactic acid are measured to be 2.79 and 0.0048 at 30 GHz, respectively. Focusing ability of the lens is studied using full-wave simulation. The lens is fabricated using a table-top commercial fused deposition modelling printer. The surface roughness, step heights, and radii of each zone are measured and verified using a 3D optical profilometer. Impact of the 3D-printed limitation on performance of the device is discussed. The gain of the fabricated prototype is measured, in conjunction with a horn antenna, in an anechoic chamber. Pattern measurement results illustrate 6.6 dB gain enhancement at broadside at 30 GHz. Gain enhancing behaviour is studied at three different focal lengths and frequencies of 29–31 GHz.

1 Introduction

High gain antennas are commonly required for millimetre wave (30–300 GHz) communication or other applications such as radar systems. Due to high atmospheric attenuation, the gain enhancement becomes more crucial at the millimetre wave band [1, 2]. There are several ways to achieve high gain systems including large antenna arrays or reflector antennas. One of the alternative approaches for achieving higher gain and directivity can be a lens structure collimating the electromagnetic (EM) wave to form the directive beam. Moreover, the lens structure is currently being considered as a solution of wireless power transfer (WPT) technology [3]. Harvesting and transmitting the energy in millimetre wave and far-field regions with higher efficiency are the key factors of the specification that the lens structure has to achieve.

A Fresnel lens has several advantages over conventional convex or concave lenses, especially, for WPT application. It has lower profile and less absorption loss in millimetre wave band than the other types of lens. Moreover, a Fresnel lens uses diffraction to make the phase correction and to collimate the EM wave at the focal point as compared to refraction in conventional lenses. In detail, spherical waves are compensated by using a stepwise phase correction, such as half-wave, quarter-wave, or eight-wave grooved dielectric zones [4]. Also, changing the permittivity of each zone in the lens can be one of the various methods of phase compensation. There are several ways to control the permittivity of the lens, such as making porosities on the surface of the lens [5] or using totally different material with different permittivity in each zone [6]. Contrary to traditional convex and concave lenses, a Fresnel lens can be combined with those methods to reduce profile and weight. It can achieve volumetric advantages due to its flat surface instead of an arched surface. Also, for the simplicity of fabrication, it can be realised using additive manufacturing (AM).

Often referred to as 3D printing technology, AM is the process of building 3D structures from digitally coded files. Unlike planar manufacturing techniques, it can elaborately realise 3D structures with curvatures and discrete parts. Also, 3D printing techniques can allow for fast prototyping and optimisation of the lens with low cost. However, limitation of this technology for realisation of EM structure has not been fully studied. As recently reported, AM has been studied and implemented to fabricate lenses at microwave band. In the case of [7, 8], the authors implemented the method of controlling the infill density of each zone of the lens to achieve the different permittivity. A non-planar Luneburg lens was realised, and refractive index was gradually implemented to obtain different permittivity values in [9]. The 3D-printed lens has been integrated with the helical antenna for the gain enhancement achieving the gain improvement of 4.6 dBi at 8.8 GHz [10].

In this work, we report the design, simulation, fabrication, material characterisation, and test results for planar and thin 3D-printed Fresnel lens with excellent gain enhancing ability and a short focal length. Our work has several novelties over the other studies. This paper reports measurement of the exact position of focal point with our own in-house fixture that has never been reported for similar lenses. Launching horn is integrated with the 3D-printed fixture during the gain measurements. This is used as a verification technique for simulation results. The small size of the focal length (40 mm) provides instrumentation, accuracy, and repeatability challenges, especially, when measured in the anechoic chamber. We verify the significance of choosing the distance between the lens and the antenna through the measurement using 3D fabricated in-house fixture which can manipulate the distance with a resolution of 2.5 mm. Performance degradation is shown when the location of the lens or horn is not at the focal distance. We discuss, with clarity, the concept of focusing gain and its importance in designing any Fresnel lens. Focusing gain for a lens was first was reported in [11]; however, it was implemented only in the analytical calculation. Full-wave simulation of electrically large structures with several fine features (steps) is challenging. In our design, the lens is ~12λ in diameter and 1λ in thickness. In some previous measurement setups of the lens with antenna, the relationship between the focal point of the lens and phase centre of the antenna is not properly demonstrated. The distance between the antenna under test and the lens influences the performance of the lens; hence, the measured results are altered when setting the undesired distance. The verification of the prototype using measurements is reported here. While the initial design of 3D-printed Fresnel lens was reported in [12], complete gain enhancing behaviour is included in this work. Moreover, the investigation of the 3D-printed step heights, surface roughness and radii of each cylindrical ring is critically needed to verify the accuracy of

Fig. 1 *3D schematic view of lens composed of 4 quarter wave zones and 4 step heights*
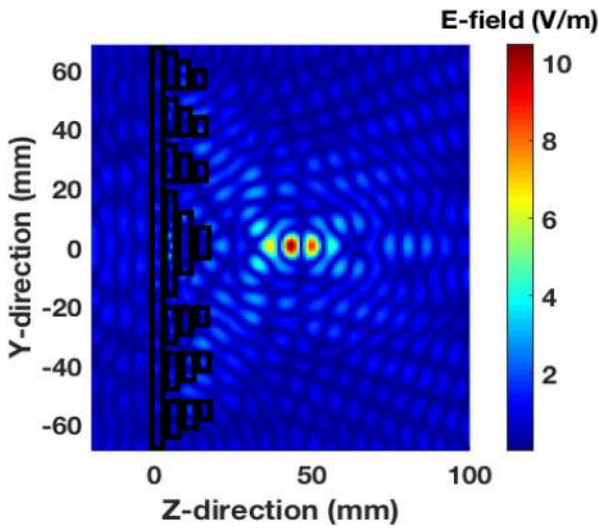

Fig. 2 *Simulated electric field on a plane perpendicular to the lens showing incident plane wave and focused beam on left and right, respectively*

fabrication. Here, we highlight the limitations of the 3D printing technology for fabrication of lens structures by reporting empirical data. The proposed fabrication process can be employed and expanded to other 3D-printed EM structures. In the millimetre wave and terahertz (THz) bands, the dielectric constant (ε_r) and the loss tangent (tan δ) of the polymer-based filament used in 3D printing is not fully known. Fabrication process can also impact the complex permittivity of the 3D-printed material depending on specific tool, temperature, or other parameters. Therefore, one needs to characterise the exact ε_r and tan δ at the operating frequency before designing a lens. The broadband measurement of the complex permittivity of the material is reported in detail.

With above differentiations in mind, this paper is organised as follows. In Section 2, we first report the design of a Fresnel lens and provide basic information on its geometry. Second, we discuss full-wave simulation results and focusing ability of the lens. Gain and focal point optimisation of the lens and phase centre of the test horn antenna are discussed. In Section 3, the measured ε_r and tan δ of polylactic acid (PLA) using a terahertz time-domain spectroscopy (THz-TDS) are reported. Results are compared to literature at the closest frequency bands to 30 GHz. This way, extrapolation approach is validated. Fabrication results, including the step height, surface roughness, and radii of each cylindrical ring in the lens, are presented in Section 4. Pattern measurement, gain enhancement, and maximum gains in the range of frequency from 29 GHz to 31 GHz are reported in Section 5. Measurement results are compared to full-wave simulation. Discussion and concluding remarks are provided in Section 6.

2 Design and simulation of Fresnel lens

2.1 Design procedure

A Fresnel lens uses diffraction as the method of phase correction. It is composed of discrete stepwise patterns that can reduce the bulkiness and the curvatures of conventional lenses. Moreover, it is light-weight and easily fabricated due to its flat surface. There are several methods to manipulate the phase, which are introduced in Section I. In this work, we implement cylindrical annular rings with single dielectric material. Fig. 1 shows the schematic 3D view of the designed Fresnel lens. Since only a single material type is employed, the fabrication process is simple and fast. Also, this approach can potentially reduce the possibility of fabrication errors as compared to fabricating vias or implementing the various material with different permittivity. The outer radius of each annular ring, R_F, is derived using [13]:

$$R_F = \sqrt{\left(\frac{n\lambda}{4}\right)^2 + \frac{2nD\lambda}{4}}, \quad n = 1, 2, \ldots, L.$$ (1)

where L is the total number of rings, D is the focal length, and λ is the wavelength. D is chosen to be 40 mm to shorten the focal length to diameter ratio. It has been shown that if the ratio of the focal length to the diameter is <0.5, which is defined as a short-focal lens, the weight and size advantages are pronounced [14]. The focal length-to-diameter ratio in our design is 0.29. Sixteen rings with a maximum radius of 69.3 mm are designed.

The step height of the cylindrical annular rings is determined using [15]:

$$T_F = \frac{\lambda}{4(k-1)}, \quad k = \sqrt{\varepsilon_r}$$ (2)

The lens is supported on a 1-mm-thick layer. Each step is 3.6 mm in height making the total thickness to be 11.8 mm or 1λ thick.

2.2 Simulation

After designing the lens, a full-wave simulation (ANSYS-HFSS) is carried out to determine and optimise the focal point and gain. The precise location of the focal point is crucial in the gain-enhancing performance of the lens. This is also verified through the measurement in Section 5. The geometry of the antenna determines interactions between a spherical EM wave forming the focal point and the plane wave forming a far-field pattern on the other side of the lens. One example of this interaction between the wave and the lens is illustrated in Fig. 2.

As can be seen here, the incident plane wave is excited on the left side of the lens, and the phase correction occurs at its surface. The wave is focused at 40 mm from the bottom surface of the lens. To quantify the focusing ability and clarify the focal point of the lens, we use the concept of focusing gain (FG). The focusing gain is defined here as the ratio of Poynting vectors that are on the forwarding axis [11]. In the case where incident plane wave passes through the z-axis, the ratio can be derived with the z-axial components before ($\vec{S}_c^i$) and after ($\vec{S}_c$) penetrating the lens. Thus, focusing gain is calculated as:

$$FG = \frac{\left| Re[\hat{z} \times \vec{S}_c] \right|}{\left| Re[\hat{z} \times \vec{S}_c^i] \right|}$$ (3)

After optimising the design, a maximum focusing gain of 20.3 dB is achieved at a distance of 40 mm using the full-wave simulation. Result is shown in Fig. 3. This demonstrates that the lens can collimate the EM wave at the expected location. Therefore, the phase centre of the test antenna should be located at this exact point to maximise the gain enhancement. Once the precise position of the antenna and the focal point of the lens are defined, a far-field pattern can be obtained.
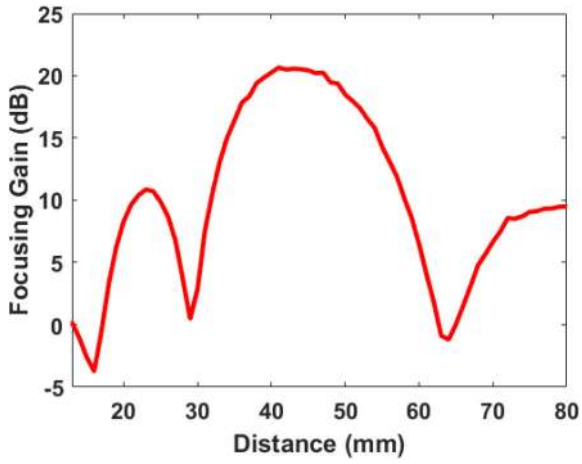
Fig. 3 *Simulation result of the focusing gain (in dB) as a function of the distance from the bottom surface of the lens*
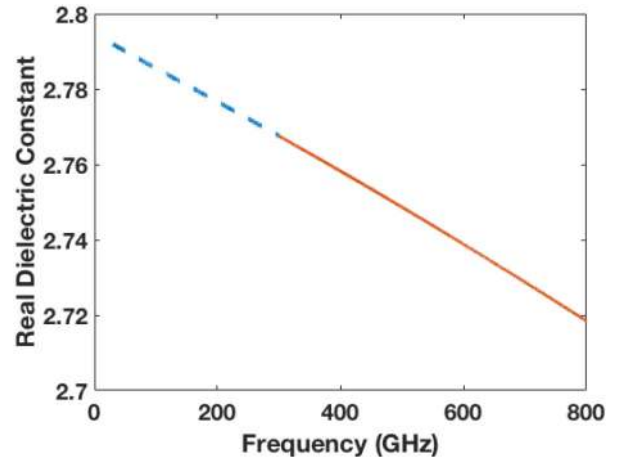

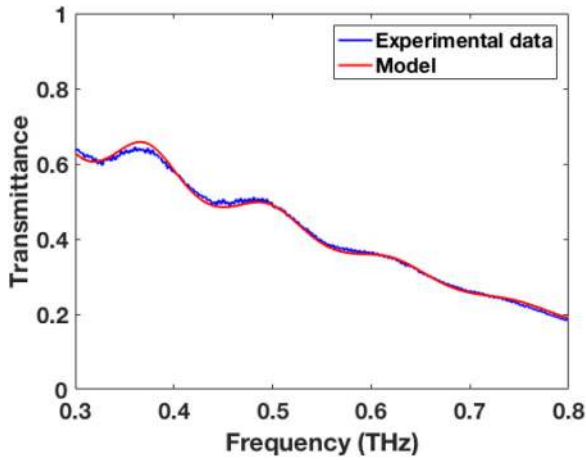**Fig. 5** *Measured real part of the complex permittivity of 0.8-mm-thick PLA sample*

Fig. 4 *Measured transmittance through 0.8-mm-thick PLA sample*
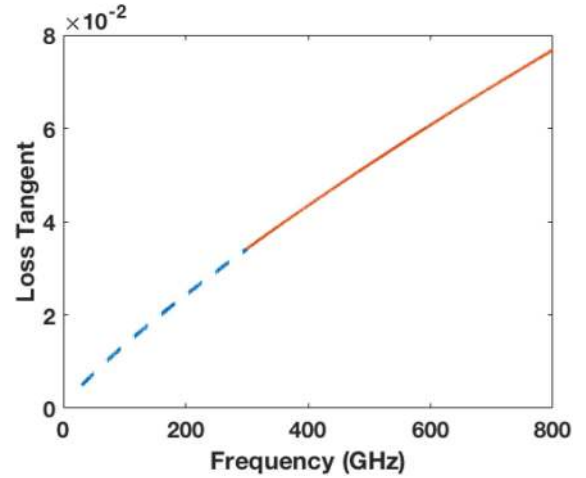

Fig. 6 *Measured loss tangent of 0.8-mm-thick PLA sample*

3 Electrical characterisation of PLA

3.1 Analytical model

Before fabricating the lens, we investigate the dielectric characterisation of PLA as it is commonly used in fused deposition modelling (FDM). As shown in (2), the permittivity of the material affects the geometry and performance of the lens. In our work, we use THz-TDS technique in transmission mode.

Several techniques, such as guided wave transmission and cavity resonance systems, have been used in the past for complex permittivity measurements [16]. However, cavity resonance systems can measure the dielectric properties only at a single frequency and sample preparation is complicated. A sample should be inserted inside the waveguide which has a limited space. Moreover, a guided wave transmission system has a narrower bandwidth than TDS system that is implemented in our work. We note that the major drawback of our approach is that the frequency range of the measurement is much >30 GHz. However, complex permittivity values for lower frequencies can be found using simple curve fitting. With the advantages of wider bandwidth and easier sample preparation, TDS system was adopted in our study. First, we set an analytical model to calculate ε_r and $\tan\delta$ from the measured transmission. Dielectric properties of polymer-based material can be analytically modelled with the Havriliak–Negami relation [17]:

$$\varepsilon_r = \varepsilon_\infty + \frac{(\varepsilon_s - \varepsilon_\infty)}{\left(1 + (j\omega\tau)^{(1-\alpha)}\right)^\beta} \qquad (4)$$

where ε_r is the real part of the permittivity, ε_s is the permittivity at lower frequency, ε_∞ is the permittivity at high-frequency limit, τ is the relaxation time of the material, and α β represent the asymmetry and broadness, respectively. Based on the measurement results, unknown parameters can be derived from the optimisation of the non-linear least square fit as we previously reported in [18].

3.2 Complex permittivity measurement setup and results

We fabricated a PLA sample (100% fill) with a thickness of 0.8 mm using a 3D-FDM printer (Ultimaker 2 + Extended). A commercial THz-TDS system (TPS Spectra 3000 from TeraView Ltd) is used to measure the phase and amplitude of the transmitted wave through the samples similar to [19, 20]. Fig. 4 shows the results of change in transmittance amplitude for the 0.8-mm-thick PLA sample in the frequency range of 0.3–0.8 THz. According to the figure, the experimental data and the analytical model are in good agreement. Phase measurement results also show close agreement with our model.

Next, the real parts of the permittivity and loss tangent of a 0.8-mm-thick PLA sample are derived and extrapolated to 30 GHz from the measurement data in Figs. 5 and 6, respectively. As shown here, the change in measured permittivity is linear function of frequency.

As illustrated in Figs. 5 and 6, ε_r and $\tan\delta$ are extrapolated with blue-dotted lines. As the range of THz-TDS measurement is from 0.3 to 0.8 THz, ε_r and $\tan\delta$ of PLA at 30 GHz are calculated with Havrilliak–Negami relation and plotted with the extrapolation. Calculated ε_r and $\tan\delta$ of PLA from the measured data are 2.79 and 0.0048 at 30 GHz, respectively. Moreover, this study of dielectric properties at millimetre wave band can be implemented to other materials. Derived values of ε_r and $\tan\delta$ are used in the full-wave simulation to achieve more accurate design. To further validate our results, we present a comparison of measured values (for ε_r and

Table 1 Comparison of dielectric characteristics of PLA measured by our group and others

| Ref. NO.	ε_r	$\tan\delta$
[21]	3.55 at 9–10 GHz (waveguide method)	−0.001 (waveguide method)
	3.47 at 9–10 GHz (probe method)	0.073 (probe method)
[22]	2.86 at 40 GHz	0.013 at 40 GHz
	2.84 at 60 GHz	0.015 at 60 GHz
	(both averages with waveguide method)	(both averages with waveguide method)
[23]	2.54 at 40 GHz	0.02 at 40 GHz
	2.52 at 60 GHz	0.02 at 60 GHz
	(both with coplanar waveguide method)	(both with coplanar waveguide method)
Our work	2.79 at 30 GHz	0.0048 at 30 GHz
	2.79 at 40 GHz	0.006 at 40 GHz
	2.78 at 60 GHz	0.009 at 60 GHz
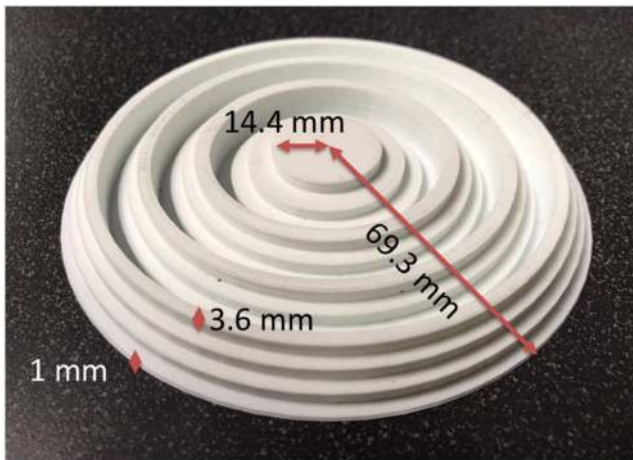
Fig. 7 *Fabricated Fresnel lens prototype*

Fig. 8 *Measured 3D profile between two Fresnel rings using an optical profilometer*

tanδ of PLA) with literature. Table 1 illustrates the dielectric properties of PLA from [21–23] as well as our work using THz-TDS explained above. Although different techniques (probe, waveguide, THz Spectroscopy) are employed in each work, as Table 1 shows, the values of ε_r and tanδ are closely matching.

It is certainly desirable to measure the complex permittivity of PLA or other 3D-printed material at the exact frequency of operation which is 29–31 GHz in our case. However, due to instrumentation limitations, this type of measurement is often not possible. As was shown in [19] and other works, the change in the
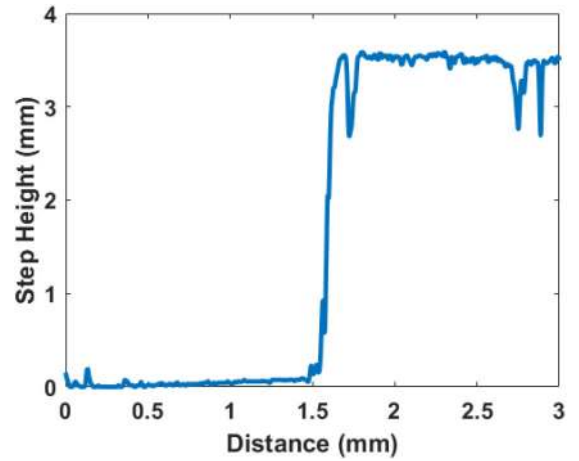

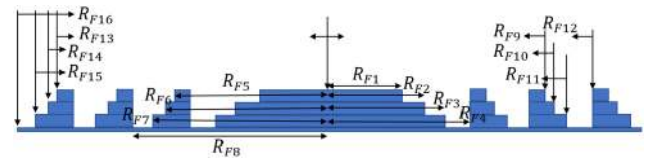**Fig. 9** *Measured step height between two annular rings showing 3.4 mm*

Fig. 10 *Cross-section of the fabricated lens with each radius, R_{FN} (N = 1, 2,...,16)*

real and imaginary part of permittivity for this material is linear with frequency in the millimetre wave band. Therefore, extrapolation provides an accurate estimate.

4 Fabrication results

4.1 Fabrication

To fabricate the lens, we employ the same FDM printer (Ultimaker 2 + Extended) used earlier for complex permittivity study. The size of the spray-head is 0.4 mm. From the datasheet, the layer resolution of the printer using 0.4 mm-nozzle is from 0.2 to 0.02 mm. The fabrication of a lens with 100% filling takes 23 h to be completed. The final fabricated prototype is shown in Fig. 7.

4.2 Geometric verification

Upon completion of the lens fabrication, we measure the step heights and radii of the cylindrical ring using a non-contact optical profilometer (Zeta-20 from KLA-Tencor) and a digital calliper, respectively. The field of view for the measurement using the profilometer is 3.30 mm × 2.48 mm. Step height resolution of the tool is 5.7 μm. Using this system, we also measure the surface roughness of the lens. Fig. 8 shows the 3D view and profile between two Fresnel rings.

Fig. 9 shows 2D scanning results of a ring. The average step height across the lens is measured to be 3.4 mm compared to the designed value of 3.6 mm. The average surface roughness, R_a, is measured to be 0.4 mm or 0.04λ among the 247 points on the surface. To calculate this value, we use the arithmetical mean deviation of each measured point (y_k) defined as,

$$R_a = \frac{1}{N}\sum_{k=1}^{N}|y_k| \qquad (5)$$

Second, the desired radii of the cylindrical rings from Section 2 are compared with the radii measured with the digital calliper. A cross-section of the lens is shown in Fig. 10. Table 2 shows the calculated and measured average of each radius. As can be seen from the table, the fabricated rings have shorter radii than modelled based on (1) with the range of discrepancy from 0.05 to 0.3 mm. In terms of relative error, we observe 0.3 to 0.5%. We can conclude that the fabricated lens has a z-axial error of ±0.4 mm, while the x- and y-axial errors are from −0.05 to −0.3 mm. The direction of

Table 2 Comparison between the designed and the measured (average) radii of the fabricated rings

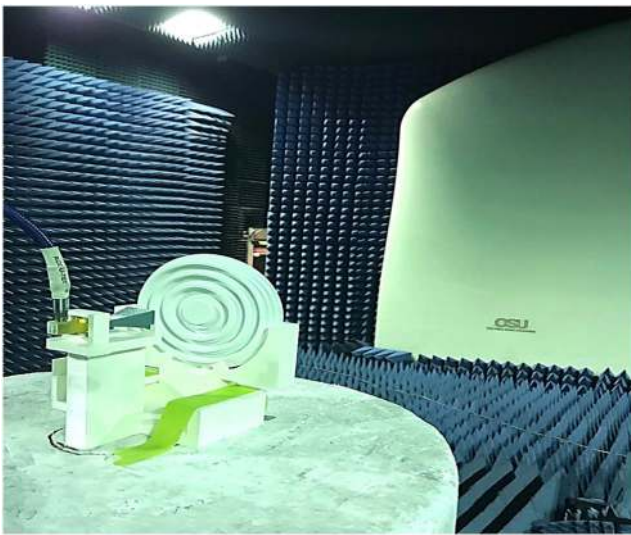|	Designed, mm	Measured, mm
R_{F1}	14.4	14.35
R_{F2}	20.6	20.55
R_{F3}	25.6	25.5
R_{F4}	30.0	29.75
R_{F5}	34.0	33.9
R_{F6}	37.7	37.5
R_{F7}	41.3	41.2
R_{F8}	44.7	44.4
R_{F9}	48.0	47.9
R_{F10}	51.2	51.0
R_{F11}	54.4	54.2
R_{F12}	57.4	57.1
R_{F13}	60.5	60.3
R_{F14}	63.4	63.2
R_{F15}	66.4	66.2
R_{F16}	69.3	69.2

Fig. 11 *Holistic view of the measurement setup in an anechoic chamber. The lens and antenna are mounted on a 3D-printed holder (fixture)*
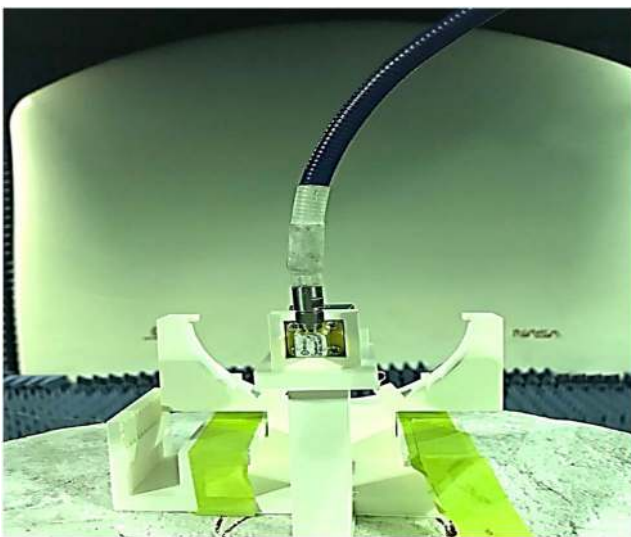

Fig. 12 *Close-up view of the measurement setup without the lens in an anechoic chamber*
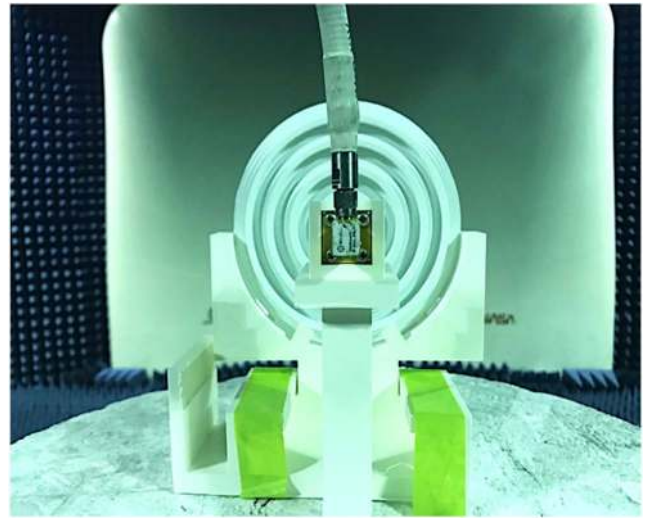

Fig. 13 *3D-printed fixture ensures that the lens is located at the focal point of the antenna without tilting or misalignment*

deposition (*z*-axis) has more critical error of fabrication than any other directions (*x*- and *y*-axis). As mentioned in Section IV-A, the layer resolution of the nozzle (0.4 mm) is from 0.2 to 0.02 mm. Measured *x*-, *y*-, and *z*-axial errors are in the range of given layer resolution from the datasheet. We directly verify that the prototype has a close tolerance in all three axes. Maximally, 0.2 mm (0.02λ) of discrepancy in *z*-axis and 0.1 mm (0.01λ) of discrepancy in *x*- and *y*-axes have been achieved. However, these discrepancies cannot affect the results, demonstrated next in Section V.

5 Measurement setup and results

5.1 Measurement setup

The measurement setup is shown in Figs. 11–13. A standard gain horn (Narda V637) operating at 26.5 to 40 GHz (Ka-band) is used as a transmitting antenna in an anechoic chamber. In addition, 3D fabricated in-house fixture with PLA using the same FDM printer is employed for precise positioning of the horn at the focal point. This fixture also ensures the perpendicular positioning of the lens to the EM wave. As a part of this fixture, we included a built-in Vernier scale to measure the exact distance between the lens and the horn during measurements. Cursor-to-cursor distance is 2.5 mm. To verify the impact of distance to performance, ±5 mm-distance manipulation (35, 40 and 45 mm) from the aperture of the horn and the bottom surface of the lens is carried out.

5.2 Measurement results

The simulation and measurement results for the horn antenna without the lens are shown in Fig. 14. This step is used as a baseline and for verification only. The simulated maximum gain of the horn is 16.2 dBi as compared to the measured value of 15.9 dBi. These show good agreement.

Gain enhancement of the Fresnel lens is measured next in the anechoic chamber. The simulated and measured results of the same horn with the lens are shown in Fig. 15. As expected, the gain of the horn antenna when placed on the focal point of the lens is enhanced. We note that, using full-wave simulation, the phase centre of the horn at 30 GHz is estimated to be 5 mm from the front aperture of the horn. The simulated and measured gain are 22.7 and 22.5 dBi, respectively. Moreover, the simulated and measured half power beam width (HPBW) of the antenna when using the lens are 7° and 8°, respectively. This demonstrates that the antenna can obtain more directive beam pattern when used together with the fabricated lens. Gain enhancing performance of the lens is extracted from the patterns, resulting in 6.5 dBi for the simulation and 6.6 dBi for the measurement.

Figs. 16 and 17 show the radiation patterns of the horn with the lens at 29 and 31 GHz, respectively. Measurement and simulation results at both frequencies are closely matched. HPBW at 29 and
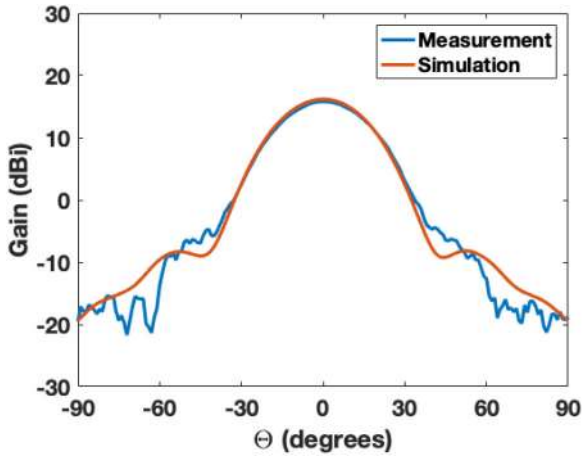
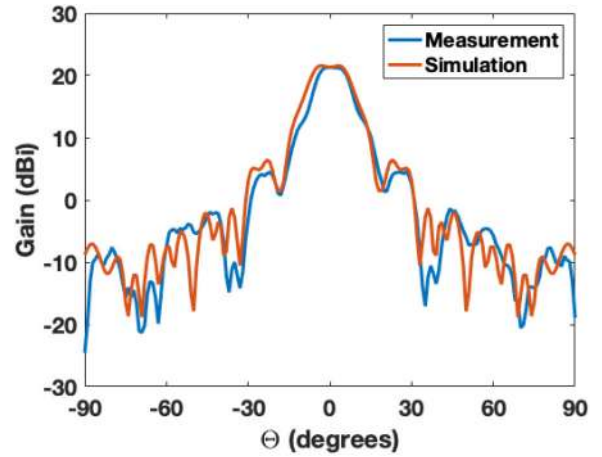**Fig. 14** *Simulated and measured radiation patterns of the horn without the lens at 30 GHz*

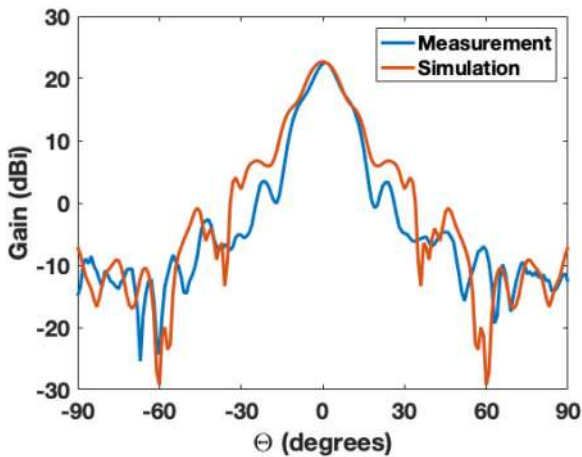**Fig. 15** *Simulated and measured radiation patterns of the horn with the lens at 30 GHz*

Fig. 16 *Simulated and measured radiation patterns of the horn with the lens at 29 GHz*

Fig. 17 *Simulated and measured radiation patterns of the horn with the lens at 31 GHz*
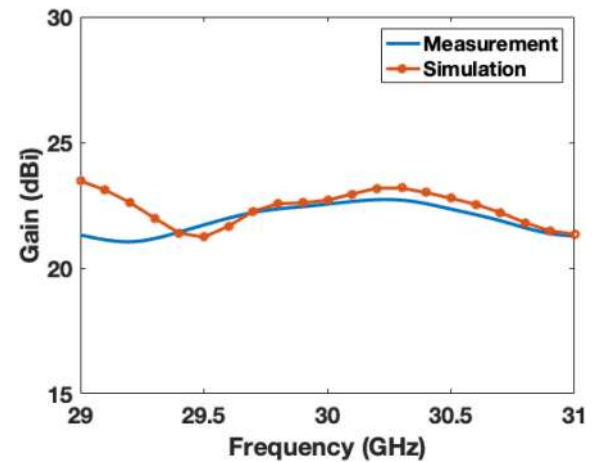

Fig. 18 *Simulated and measured maximum gains of the horn with the lens (with the step size of 10 MHz) in the range of 29 to 31 GHz*
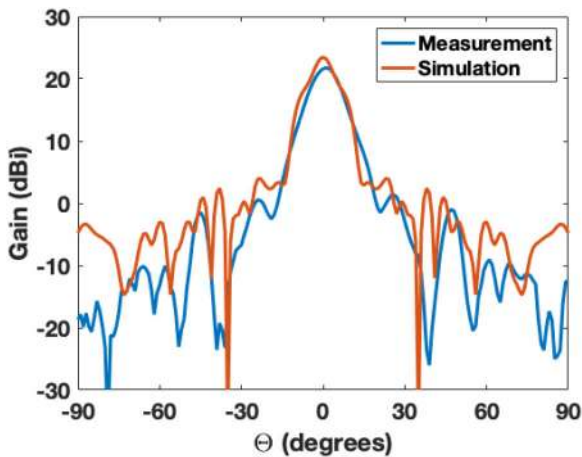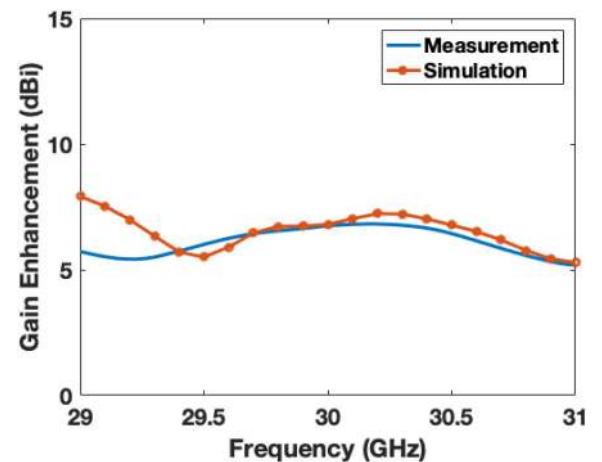

Fig. 19 *Simulated and measured gain enhancement of the horn with the lens (with the step size of 10 MHz) in the range of 29 to 31 GHz*

31 GHz are 9° and 11°, respectively, which are broader compared to the 30 GHz performance. The fabricated lens is designed at 30 GHz with (1) and (2), which are frequency-dependent. Therefore, the performance of the lens is degraded in 29 and 31 GHz. In Figs. 18 and 19, the maximum gains and gain-enhancing performance of the fabricated lens (measurement) and modelled lens (simulation) are shown. Measurement frequency resolution is 10 MHz. The targeting ability of the fabricated lens in terms of the operating frequency can also be demonstrated with these results. As shown by (1) and (2), the performance of the Fresnel lens is frequency-dependent. As a result, the geometry of the lens was

modelled at 30 GHz and expected to perform properly at this frequency only. Figs. 18 and 19 illustrate that peak gains and gain-enhancing performance of the fabricated and modelled lens are generally in good agreement. Moreover, in terms of HPBW and maximum gain, the best measured results are achieved ~at 30 GHz.

With respect to the peak gain, the simulated result at 29 GHz has a maximum value of 23.4 dBi, which is 0.7 dBi higher than the gain at 30 GHz. However, peak gain does not contain all the necessary information. As shown in Fig. 16, HPBW is 2° broader than the beam at 30 GHz in both simulation and measurement

results. Therefore, we conclude that, as expected, the best performance is obtained at 30 GHz.

Depending on the application, if optimum beam pattern is not the primary driver, one may use this lens at other frequencies. For instance, our lens has a relatively stable gain enhancement over the frequency range of 29 to 31 GHz for both simulated and measured results. In this band, the gain enhancement of 5.4 dBi up to 6.8 dBi are observed in both simulation and measurement results. In conclusion, from the pattern measurements, we can verify our lens' ability of enhancing the gain of the antenna and forming the directive beam.

For the verification of the focal point, we manipulated the distance between the aperture of the horn and lens by ±5 mm. As mentioned earlier, a 3D-printed fixture (stage) with a Vernier scale was fabricated for precise positioning of the lens and the horn. Measurement results at 30 GHz are shown in Fig. 20. The maximum gain appears at the desired distance (40 mm) between
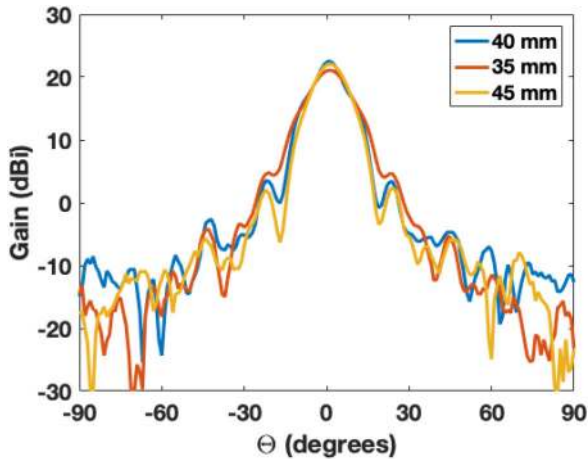

Fig. 20 *Measured radiation patterns (at 30 GHz) of the horn with the lens at the various distances (35, 40, and 45 mm)*
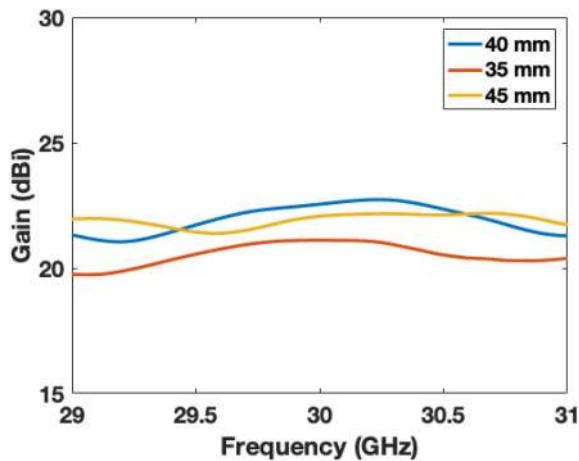

Fig. 21 *Measured maximum gains of the horn with the lens with respect to the frequency at the various distances (35, 40, and 45 mm)*

the lens and the horn. At the distances of 35 and 45 mm between the lens and the horn, 22 and 21 dBi of gains are achieved, respectively. Measured maximum gains as a function of frequency and distance are shown in Fig. 21. Approximately, at 30 GHz, larger gains are obtained at the desired distance than any other gains at the mismatched values of distance. From the three sets of measurements, we can verify that the focal length of the fabricated lens matches well with the designed value and the distance between the horn and the lens is properly set up in our experiment.

Table 3 shows comparison of the lens discussed here and several examples of lenses fabricated with AM from the literature. Our lens has a lower profile compared to other lenses operating in lower frequency bands. In addition, the information of gain enhancing performance is ambiguous in other works. However, we accurately report the gain enhancement using radiation patterns and define the exact value of how much the antenna performance is improved with respect to the gain and HPBW. Finally, our prototype is the only one at Ka-band using AM, and detailed process of manufacturing the millimetre wave lens is proposed in this work.

6 Discussion and conclusion

We note that the tested Fresnel lens is expected to increase undesired cross-polarisation as well as co-polarisation gain. This is due to the symmetry in the geometry. Depending on the application, this can be compensated by using the asymmetric design in the direction of cross-polarisation. We also note that, due to Fresnel lens principles of operation, the lens needs to be properly oriented as compared to the receiving (or transmitting) antenna. We have addressed this issue by building an in-house 3D-printed fixture. In practice, this precise positioning may create limitations for certain applications.

Moreover, the lens has disadvantages of lower efficiency and narrow bandwidth. Calculated actual physical area of the lens, which has 40 mm focal length and *f*-number of 0.29 is 0.014 m2. Effective aperture of antenna which has measured gain of 22.46 dBi at 30 GHz is 0.0014 m2. Therefore, the prototype has an efficiency of 10%, which is lower than other types of lens. Due to the shape of the grooved structure, there are shadow blockage effects on the aperture efficiency of Fresnel lens [27] degrading the overall efficiency. Also, with a small focal length to diameter ratio, the shadow blockage effects are more pronounced. To avoid the shadow blockage, multi-dielectrics can be used to fabricate the lens. However, this method makes the fabrication process complicated. Moreover, by using large focal length to diameter ratio, the degradation due to the shadow blockage effect can be suppressed. Although there are trade-offs between the simple fabrication and degradation of the performance, we focus on the fast and simple fabrication using AM.

In this paper, we presented the design, fabrication, and measurement of a low-profile Fresnel lens. Electrical properties of PLA material were measured using a THz-TDS system, and they are found to be 2.79 and 0.0048, respectively. After the measurement, full-wave simulation was used to optimise the geometry and set up the desired location of the focal point. Geometries including step heights, surface roughness, and radii of each cylindrical ring of the fabricated lens, all of which were

Table 3 Comparison of Fresnel lens fabricated using additive manufacturing

Ref. NO.	Phase correction method	Operating frequency, GHz	Size	Peak gain, dBi	Gain enhancement, dB
[24]	Graded index	8–12	Radius: 104 mm (3.5λ), Thickness: 20.5 mm (0.7λ)	7.3–12.8	—
[10]	Grooved	8–12	Radius: 80 mm (2.7λ), Thickness: 53 mm (1.7λ)	12.9	4.6
[25]	Graded index	12–18	Radius: 120 mm (6λ), Thickness: 18.5 mm (0.9λ)	16–24	—
[26]	Perforated	55–65	Radius: <163.5 mm (31.4λ), Thickness: 3 mm (1.7λ)	34	12
our work	Grooved	29–31	Radius: 69 mm (6.9λ), Thickness: 11.8 mm (1.2λ)	21–23.4	5.4–6.8

investigated and found to be in good agreement with our design. Average surface roughness was measured to be 0.4 mm or 0.04λ and found to be insignificant for the operation of the lens at 30 GHz, though would matter greatly at higher frequencies.

Using several measurements, we have experimentally verified the operation of the lens. Specifically, the focal point of the lens was investigated at the desired distance of 40 mm between the bottom surface of the lens and the phase centre of the horn. Furthermore, the maximum gain of 22.5 dBi at 30 GHz appeared at this focal point, while lower gains were achieved at other distances (35 and 45 mm). Enhancement in the realised gain was measured in the anechoic chamber and compared to the simulation. Pattern measurement results illustrated 6.6 dBi enhancement in co-polarisation gain. We demonstrated the feasibility of employing all-dielectric 3D-printed Fresnel lens in millimetre wave band. Our fabricated lens enables imaging systems, satellite communication, or WPT technology. The latter has an application including sensors, electric vehicle charging, and RF identification.

7 Acknowledgments

8 References

[1] Rappaport, T.S., Murdock, J.N., Gutierrez, F.: 'State of the art in 60-GHz integrated circuits and systems for wireless communications', *Proc. IEEE*, 2011, **99**, (8), pp. 1390–1436

[2] Rangan, S., Rappaport, T.S., Erkip, E.: 'Millimeter wave cellular wirelss networks: potentials and challenges', *Proc. IEEE*, 2014, **102**, (3), pp. 366–385

[3] Gonçalves, R., Carvalho, N.B., Pinho, P.: 'Wireless energy transfer: dielectric lens antennas for beam shaping in wireless power-transfer applications', *C. R. Phys.*, 2017, **18**, (2), pp. 78–85

[4] Rodriguez, J.M., Hristov, H.D., Grote, W.: 'Fresnel zone plate and ordinary lens antennas: comparative study at microwave and terahertz frequencies'. Proc. 41st Eur. Microw. Conf., Manchester, UK, October 2011, pp. 894–897

[5] Petosa, A., Ittipiboon, A.: 'Design and performance of a perforated dielectric fresnel lens', *IEE Proc. Microw., Antennas Propag.*, 2003, **150**, (5), pp. 309–314

[6] Hristov, H.D., Rodriguez, J.: 'Design equation for multidielectric fresnel zone plate lens', *IEEE Microw. Wireless Compon. Lett.*, 2012, **22**, (11), pp. 574–576

[7] Zhang, S.: '3D printed dielectric fresnel lens'. 2016 10th Eur. Conf. Antennas Propagation, (EuCAP 2016), Davos, Switzerland, April 2016, pp. 3–5

[8] Zhang, S., Vardaxoglou, Y., Whittow, W., *et al.*: '3D-printed flat lens for microwave applications'. 2015 Loughborough Antennas Propag. Conf. (LAPC 2015), Loughborough, UK, November 2015, pp. 31–33

[9] Kubach, A., Shoykhetbrod, A., Herschel, R.: '3D printed luneburg lens for flexible beam steering at millimeter wave frequencies'. 2017 47th European Microwave Conf. (EuMC), Nuremberg, Germany, October 2017, pp. 787–790

[10] Farooqui, M.F., Shamim, A.: '3-D inkjet-printed helical antenna with integrated Lens', *IEEE Antennas Wirel. Propag. Lett.*, 2017, **16**, pp. 800–803

[11] Reid, D.R., Smith, G.S.: 'A full electromagnetic analysis of grooved-dielectric fresnel zone plate antennas for microwave and millimeter-wave applications', *IEEE Trans. Antennas Propag.*, 2007, **55**, (8), pp. 2138–2146

[12] Jeong, K.H., Ghalichechian, N.: 'Design, fabrication and measurement of a millimeter wave fresnel Lens using additive manufacturing'. IEEE Int. Symp. on Antennas and Propagation & USNC/URSI National Radio Science Meeting., Boston, MA, 2018, pp. 1879–1880

[13] Hristov, H.D.: '*Fresnel zones in wireless links, zone plate lenses, and antennas*' (Artech House, Boston, MA, USA, 2000)

[14] Hristov, H.D., Rodriguez, J., Grote, W.: 'The grooved dielectric fresnel zone plate: effective THz lens and antenna', *Microw. Opt. Technol. Lett.*, 2012, **54**, pp. 1343–1348

[15] Hristov, H.D., Herben, M.H.A.J.: 'Millimeter-wave fresnel-zone plate lens and antenna', *IEEE Trans. Microw. Theory Tech.*, 1995, **43**, (12), pp. 2779–2785

[16] Tereshchenko, O.V., Buesink, F.J.K., Leferink, F.B.J.: 'An overview of the techniques for measuring the dielectric properties of materials'. 2011 XXXth URSI General Assembly and Scientific Symp., Istanbul, 2011, pp. 1–4

[17] Havriliak, S., Negami, S.: 'A complex plane representation of dielectric and mechanical relaxation process in some polymers', *Polymers. (Basel)*, 1967, **8**, pp. 161–210

[18] Ghassemiparvin, B., Ghalichechian, N.: 'Broadband complex permittivity measurement of paraffin films at 26 GHz–1 THz using time domain spectroscopy'. IEEE Int. Symp. on Antennas and Propagation & USNC/URSI National Radio Science Meeting., San Diego, CA, 2017, pp. 887–888

[19] Ghassemiparvin, B., Ghalichechian, N.: 'Permittivity and dielectric loss measurement of paraffin films for mmw and THz applications'. 2016 Int. Work. Antenna Technol. iWAT 2016, Cocoa Beach, FL, 2016, pp. 48–50

[20] Ghassemiparvin, B., Ghalichechian, N.: 'Complex permittivity measurement of paraffin phase-change material at 26 GHz–1 THz using time domain spectroscopy', *Int. J. Infrared Millim. Waves*, 2019, **40**, (2), pp. 210–218

[21] Huber, E., Mirzaee, M., Bjorgaard, J., *et al.*: 'Dielectric property measurement of PLA'. 2016 IEEE Int. Conf. on Electro Information Technology (EIT), Grand Forks, ND, 2016, pp. 0788–0792

[22] Felício, J.M., Fernandes, C.A., Costa, J.R.: 'Complex permittivity and anisotropy measurement of 3D-printed PLA at microwaves and millimeter-waves'. 2016 22nd Int. Conf. on Applied Electromagnetics and Communications (ICECOM), Dubrovnik, 2016, pp. 1–6

[23] Boussatour, G., Cresson, P., Genestie, B., *et al.*: 'Dielectric characterization of polylactic acid substrate in the frequency band 0.5–67 GHz', *IEEE Microw. Wirel. Compon. Lett.*, 2018, **28**, (5), pp. 374–376

[24] Zhang, S., Whittow, W., Vardaxoglou, Y.: '3D-printed fresnel zone plate lens'. 2016 Int. Symp. on Antennas and Propagation (ISAP), Okinawa, 2016, pp. 88–89

[25] Zhang, S., Vardaxoglou, Y., Whittow, W., *et al.*: '3D-printed graded index lens for RF applications'. 2016 Int. Symp. on Antennas and Propagation (ISAP), Okinawa, 2016, pp. 90–91

[26] Pourahmadazar, J., Sahebghalam, S., Abazari Aghdam, S., *et al.*: 'A millimeter-wave fresnel zone plate Lens design using perforated 3D printing material'. 2018 IEEE MTT-S Int. Microwave Workshop Series on Advanced Materials and Processes for RF and THz Applications (IMWS-AMP), Ann Arbor, MI, 2018, pp. 1–3

[27] Petosa, A., Ittipiboon, A.: 'Shadow blockage effects on the aperture efficiency of dielectric fresnel lenses', *IEE Proc. Microw. Antennas Propag.*, 2000, **147**, (6), pp. 451–454